Supporting Information for "Historical changes and reasons for model differences in anthropogenic aerosol forcing in CMIP6"

Stephanie Fiedler[1,2], Twan van Noije[3], Christopher J. Smith[4,5], Olivier Boucher[6], Jean-Louis Dufresne[7], Alf Kirkevåg[8], Dirk Olivié[8], Rovina Pinto[9], Thomas Reerink[3], Adriana Sima[7], Michael Schulz[8]

[1]GEOMAR Helmholtz Centre for Ocean Research Kiel, Kiel, Germany

[2]Faculty of Mathematics and Natural Sciences, Christian-Albrechts-University of Kiel, Germany

[3]Royal Netherlands Meteorological Institute, De Bilt, The Netherlands

[4]University of Leeds, Priestley International Centre for Climate, Leeds, United Kingdom

[5]International Institute for Applied Systems Analysis, Energy, Climate and Environment Program, Laxenburg, Austria

[6]Institut Pierre-Simon Laplace, Sorbonne Université / CNRS, Paris, France

[7]Laboratoire de Météorologie Dynamique (LMD)/Institut Pierre Simon Laplace (IPSL), Sorbonne Université/CNRS/École Normale Supérieure/École Polytechnique, Paris, France.

[8]Norwegian Meteorological Institute, Oslo, Norway

[9]University of Cologne, Institute of Geophysics and Meteorology, Cologne, Germany

Contents of this file

0094-8276/23/$5.00

Text S1.

1. Models contributing to RFMIP-SpAer

The EC-Earth model configuration participating in RFMIP-SpAer is EC-Earth3, the base version of the suite of model configurations contributing to CMIP6 (Döscher et al., 2022). It consists of an atmosphere and land surface model adapted from cycle 36r4 of the European Centre for Medium-Range Weather Forecasts (ECMWF) Integrated Forecasting System (IFS), coupled to the physical ocean and sea-ice model from NEMO3.6 (Rousset et al., 2015). The atmosphere is resolved at spectral truncation T255 and reduced Gaussian grid N128 (corresponding to 78 km at the equator) using 91 vertical levels; the ocean at the tripolar ORCA1 grid (1 degree at the equator) using 75 levels. Tropospheric aerosols are prescribed using MACv2-SP in combination with a monthly climatology of pre-industrial aerosol optical properties and concentrations representative for the year 1850. This climatology was produced in an offline simulation of TM5, the atmospheric chemistry and aerosol component of EC-Earth3-AerChem (van Noije et al., 2021). Cloud droplet number concentrations are calculated from the pre-industrial aerosol number and mass concentrations following the activation scheme from Abdul-Razzak and Ghan (2000), and modified by the factor η_N provided by MACv2-SP. In EC-Earth3, both the cloud droplet effective radius and the rate of autoconversion of cloud liquid to rain depend on N (e.g., Wyser et al., 2020; Döscher et al., 2022). Consequently, the anthropogenic aerosol forcing in EC-Earth3 includes a contribution from the cloud lifetime or the second indirect effect.

IPSL-CM6A-LR is the sixth version of the IPSL climate model (Boucher et al., 2020) composed of the LMDZ6A atmospheric model (Hourdin et al., 2020), the NEMO v3.6 model in its eORCA1 configuration, and the ORCHIDEE v2.0 model (Boucher et al., 2020). The model resolution is 144×142 gridpoints and 79 layers for the atmosphere and $1^\circ \times 1^\circ$ and 75 layers for the ocean. The radiation transfer parameterizations in LMDZ are from the RRTM code (Mlawer et al., 1997), based on a k-correlated scheme with 16 spectral bands in the longwave, and a revised version of the code from Fouquart and Bonnel (1980) with 6 wavebands in the shortwave part of the spectrum. The surface albedo was also updated over the ocean (Séférian et al., 2018) and over land based on a tuning of the albedo of individual plant functional types (PFT) so as to match the observed MODIS surface albedo. The aerosol properties are first computed at 24 wavelengths between 0.25 and 4 μm and then weighted with a typical spectral distribution of solar radiation at the surface to obtain properties over the 6 wavebands of the SW radiative transfer code. The first indirect effect is restricted to liquid clouds and to the liquid fraction of mixed clouds (i.e., ice cloud properties do not depend on aerosol properties and concentrations). The cloud droplet number concentration (N) is computed from the sum of accumulation-mode soluble aerosols with a modified empirical law following Boucher and Lohmann (1995) and can have values between 10 and 1000 cm^{-3}. The effective cloud droplet radius is computed from the cloud liquid water content and the N, with a minimum value of 5 μm. The optical properties of liquid clouds as a function of effective cloud droplet radius and liquid water content are those of the radiative scheme as they were implemented in the ECMWF model. When configured to use the MACv2-SP scheme, the N is computed from the pre-industrial aerosol monthly climatology and then scaled by η_N from MACv2-SP, and the model uses prescribed anthropogenic aerosol properties from MACv2-SP.

MPI-ESM1.2-LR is the low-resolution configuration of the Max-Planck-Institute for Meteorology Earth System Model version 1.2 for use in CMIP6 (Mauritsen et al., 2019). The atmospheric model component is ECHAM6.3 which uses the radiation transfer parameterization PSrad (Stevens et al., 2013). Tests of PSrad as an offline radiative transfer kernel for idealized aerosol cases described by Halthore et al. (2005) and Randles et al. (2013) indicated a similar performance of PSrad as for other radiation transfer parameterization schemes for the transmitted shortwave radiation, compared to accurate line-by-line calculations (not shown). MPI-ESM1.2 uses the aerosol parameterization MACv2-SP (Stevens et al., 2017; Fiedler et al., 2017) as a standard for representing anthropogenic aerosols. The implementation of MACv2-SP is in the shortwave radiation transfer parameterization to induce aerosol effects on radiation and a Twomey effect. Optical properties of natural tropospheric aerosols are prescribed as annually repeating monthly climatology. These are taken from the MPI-M aerosol climatology (Kinne et al., 2013).

NorESM2-LM is the second generation Norwegian Earth System Model configured with 2-degree horizontal resolution for the atmosphere and land components, and 1-degree for the ocean component, and 32 vertical levels (Seland et al., 2020). NorESM2 is based on CESM2.1 (Danabasoglu et al., 2020), but has a different ocean component BLOM, and atmosphere component, CAM6-Nor, which is based on CAM6 (Bogenschutz et al., 2018) but with an alternative aerosol module and extended physics parameterizations. When configured to use the MACv2-SP scheme, the preindustrial (1850) aerosol, and cloud droplet properties are calculated from CAM6-Nor's own aerosol module and code for *aci*, while the changes in aerosol optical properties, and N after 1850 are calculated from MACv2-SP. The version of the MACv2-SP code we have used here is developed from the version applied in NorESM1, e.g., used in Fiedler et al. (2019), but adapted for use with the newly implemented radiation (RRTMG) and cloud microphysics (MG2) parameterization schemes. Note that NorESM2-LM contributed to other CMIP6 experiments than those for RFMIP using the configuration p2. For comparability of the ERF estimates reported by Smith et al. (2020), who had data from NorESM2-LM p1, we include in our study results for both NorESM2-LM p1 and p2.

2. RFMIP experiments

All model experiments in RFMIP-SpAer use the MACv2-SP parameterization. Anthropogenic aerosol extinction in MACv2-SP is a function of geographical position, height above ground, time, and wavelength. We use the year-to-year scaling based on country-aggregated CMIP6 emissions from the pre-industrial (1850) to present-day (2014) from Stevens et al. (2017) to determine the present-day ERF. Month-to-month changes are constrained by the annual cycle in anthropogenic aerosol optical depth (τ) from Kinne et al. (2013). More aerosols in clouds increase the number of cloud droplets, everything else being equal (Twomey, 1974).

For RFMIP-SpAer, all four models perform at least 30-year-long atmosphere-only experiments with a prescribed monthly sea-surface temperature and sea-ice climatology, which for each model is taken from a coupled pre-industrial control simulation performed as part of the CMIP6 experiments (Eyring et al., 2016) for the Diagnostic, Evaluation, and Characterization of Klima (DECK). The *piClim-control* experiment uses pre-industrial conditions for the year 1850 and provides the baseline for calculating the ERF for the models. In this study, we use experiments that have the same setup as for *piClim-control* but with one or more anthropogenic perturbations added.

For RFMIP-SpAer, experiments with annually repeating monthly aerosol data from MACv2-SP were performed, with the setup of *piClim-control* but adding aerosols of 2014 from MACv2-SP (*piClim-spAer-aer*), and with the setup of *piClim-spAer-aer* plus all other anthropogenic perturbations of 2014 (*piClim-spAer-anthro*).

All four participating models in RFMIP-SpAer completed the *piClim* simulations. Some of the models produced several simulations to create data for more than 30 years for *piClim-spAer-aer*. More simulated years allowed us to strongly reduce the influence of model-internal variability on the magnitude of the ERF estimate that arises from different weather sequences in models.

Model-internal variability in the radiation budget affects the precision of the aerosol ERF and total anthropogenic ERF (Figure S1), even when the aerosol representation is unified. An influence of model-internal variability on ERF was previously analyzed in two CMIP5 models (Forster et al., 2016) and for aerosol ERF in some of the RFMIP-SpAer models (Fiedler et al., 2019). The year-to-year standard deviations in aerosol ERF at TOA for present-day from the RFMIP-SpAer models are 0.11–0.37,Wm^{-2}, which is similar to the ones previously reported (Fiedler et al., 2019). That variability is also similar to the year-to-year standard deviations for the total anthropogenic ERF of 0.11–0.35 Wm^{-2}, with models providing more simulated decades (IPSL-CM6A-LR) typically having a better precision in present-day ERF than those with few decades of output (NorESM2-LM p1, Figure S1).

We performed double-call diagnostics for the instantaneous radiative forcing of anthropogenic aerosols ($\mathcal{I}$) and computed the net contribution from rapid adjustments to aerosol radiative effects ($\mathcal{A}$). The diagnostic calls were in the *piClim-spAer-aer* simulations of MPI-ESM1.2, and in *piClim-spAer-anthro* of IPSL-CM6A. MPI-ESM1.2, NorESM2, and EC-Earth3 were previously evaluated regarding their $\mathcal{A}$ and $\mathcal{I}$ for the similar anthropogenic aerosol pattern of 2005. We, therefore, repeat here the diagnostic in MPI-ESM1.2 for 2014 only to have the results for identical years in comparison with IPSL-CM6A.

For comparison to RFMIP-SpAer, we use RFMIP-ERF experiments with models using their native aerosol representation. We use the experiments *piClim-aer*, *piClim-anthro*, and *piClim-control*, which have analogous setups as in RFMIP-SpAer. The standard parameterization for anthropogenic aerosols in EC-Earth3 and MPI-ESM1.2 is MACv2-SP, such that *piClim-aer* and *piClim-SpAer-aer* are identical for these two models. We, therefore, select similar Earth system models but with different aerosol treatments, namely MPI-ESM1.2-HAM for comparison to MPI-ESM1.2, and EC-Earth3-AerChem for EC-Earth3. Note that components other than the aerosols between MPI-ESM1.2 and MPI-ESM1.2-HAM, and EC-Earth3 and EC-Earth3-AerChem additionally differ, e.g., EC-Earth3-AerChem also has interactive chemistry and therefore differs in more aspects than just the representation of aerosols.

The *piClim* experiments in RFMIP were perceived as simple to encourage modeling centers to participate (Pincus et al., 2016). Other methods exist to calculate radiative forcing (e.g., see overview in Fiedler et al., 2023) including nudged experiments (Kooperman et al., 2012).

We also use thirteen RFMIP-ERF transient atmosphere-only experiments from 1850 to 2014 for decomposing the total ERF into anthropogenic ERF (experiments *piClim-histall* and *piClim-histnat*) and aerosol ERF (experiment *piClim-histaer*), shown in Figure 1. The contributing models are listed in Table S1 along with the trends in aerosol and total ERF for 1930–1960 and 2000–2014 to characterize model differences. Note that not all models provided all historical experiments, such that we can not report all trends in ERF for all models. We further assess the present-day (2014) aerosol radiative effects in the full ensemble of available *piClim-aer* experiments in RFMIP-ERF, listed in Table S2. The ensemble includes now five models and one model configuration that became newly available after the publication by Smith et al. (2020).

3. Decomposition of processes in aerosol forcing

We calculate the effective radiative effects ($\mathcal{F}$) as the change in the net radiation flux, F, to an imposed anthropogenic perturbation at fixed sea-surface temperatures (SSTs) and sea-ice concentrations. This calculation is either done at the top of the atmosphere (TOA) or at the surface. The values of $\mathcal{F}$ are calculated from the atmosphere-only experiments, namely by computing the difference in F between the experiment with the forcing agent, e.g., *piClim-aer* for the anthropogenic aerosols in 2014, and *piClim-control* of the same model. This calculation is done for the all-sky F and for the clear-sky F (cloud-free) using the last thirty years from the *piClim* experiments. The global average of $\mathcal{F}$ gives the effective radiative forcing (ERF).

For many of the *piClim-aer* and *piClim-SpAer-aer* experiments, we have diagnostic output to identify processes contributing to model differences in $\mathcal{F}$. To that end, we apply the method proposed by Ghan (2013) to all experiments providing the necessary output from diagnostic calls to the radiation transfer calculation. The contribution from instantaneous aerosol-radiation interactions (*ari*) is calculated as:

$$\mathcal{F}_{\mathrm{direct}} = \Delta(F - F_{\mathrm{af}}), \tag{1}$$

where F_{af} is the all-sky "aerosol-free" flux in *piClim-aer* and *piClim-SpAer-aer*, obtained from a diagnostic call to the radiation transfer in which aerosols have been removed. The term $\mathcal{F}_{\mathrm{direct}}$ describes the estimate of the direct radiative effects of anthropogenic aerosols. The sum of contributions associated with clouds is given by:

$$\mathcal{F}_{\mathrm{cloud}} = \Delta(F_{\mathrm{af}} - F_{\mathrm{cs,af}}) = \Delta C_{\mathrm{af}}, \tag{2}$$

describing the difference between the change in the all-sky aerosol-free flux and the clear-sky aerosol-free flux, $F_{\mathrm{cs,af}}$, equivalent to the change in the corresponding "aerosol-free" cloud radiative effects. According to this definition, $\mathcal{F}_{\mathrm{cloud}}$ accounts for instantaneous *aci*, rapid adjustment to *aci* in those models that account for them (RFMIP-ERF experiments and EC-Earth3 in RFMIP-SpAer), as well as rapid adjustments to *ari*. We refer to $\mathcal{F}_{\mathrm{cloud}}$ as cloud-mediated effects. The residual term sums other contributions not represented in $\mathcal{F}_{\mathrm{direct}}$ and $\mathcal{F}_{\mathrm{cloud}}$:

$$\mathcal{F}_{\mathrm{other}} = \Delta F_{\mathrm{cs,af}}. \tag{3}$$

Other adjustments comprise differences in the surface albedo that may arise due to changes in snow and ice cover via land-surface temperature adjustments.

For simulations in RFMIP-SpAer, we also decompose the all-sky $\mathcal{F}_{\mathrm{all}}$ into two terms:

$$\mathcal{F}_{\mathrm{all}} = f\mathcal{F}_{\mathrm{cloudy}} + (1-f)\mathcal{F}_{\mathrm{clear}}, \tag{4}$$

where f is the cloud cover fraction. The first term on the right describes cloudy-sky contributions and the second one clear-sky contributions. Moreover, we use the output from diagnostic calls of the radiation transfer calculation to obtain $\mathcal{I}$ and calculate:

$$\mathcal{A} = \mathcal{F} - \mathcal{I} \tag{5}$$

The diagnostic is limited to IPSL-CM6A-LR and MPI-ESM1.2 in RFMIP-SpAer because $\mathcal{I}$ and $\mathcal{A}$ of the 2005 anthropogenic aerosols have been previously assessed for NorESM1, EC-Earth3, and MPI-ESM1.2 (Fiedler et al., 2019). We only repeat the $\mathcal{I}$ diagnostics for the aerosol of 2014 in MPI-ESM1.2 to have a reference for the evaluation of IPSL-CM6A-LR for the same year.

We further compute the Mass Absorption Coefficient (MAC) of black carbon (BC) at 550 nm for all models that provided the necessary output. Column-integrated BC loads were not available from any model experiments. We, therefore, calculate the BC load from the 3-D BC mass mixing ratios (variable mmrbc, in kg/kg) and the air mass per unit area (variable airmass, in kg/m^2) for all model experiments that provided these variables in the output. The anthropogenic contribution to the BC load is calculated as the difference between the total present-day and pre-industrial BC loads (kg/m^2). Because the absorption aerosol optical depth (τ_{abs}) due to absorption by BC only is not available in CMIP6, we approximate the MAC of BC as the total τ_{abs} at 550 nm of all tropospheric aerosol components combined divided by the BC load. When spatially averaging the MAC one needs to apply the BC load multiplied by the area as a weighting function. The global mean MAC is thus given as the ratio of the global mean τ_{abs} divided by the global mean BC load. Again we determine the anthropogenic τ_{abs} contribution by subtracting the pre-industrial from the present-day values, and calculate the MAC of anthropogenic BC as the ratio of the anthropogenic τ_{abs} and the anthropogenic BC load. The results for the BC load and MAC of BC are listed in Table S3.

References

Abdul-Razzak, H., & Ghan, S. J. (2000). A parameterization of aerosol activation 2. multiple aerosol types. *J. Geophys. Res.*, *105*(D5), 6837–6844. doi: 10.1029/1999JD901161

Bi, D., Dix, M., Marsland, S., O'Farrell, S., Sullivan, A., Bodman, R., ... Heerdegen, A. (2020). Configuration and spin-up of ACCESS-CM2, the new generation Australian Community Climate and Earth System Simulator Coupled Model. *Journal of Southern Hemisphere Earth Systems Science*, *70*(1), 225–251. Retrieved from `https://doi.org/10.1071/ES19040`

Bogenschutz, P. A., Gettelman, A., Hannay, C., Larson, V. E., Neale, R. B., Craig, C., & Chen, C.-C. (2018). The path to CAM6: coupled simulations with CAM5.4 and CAM5.5. *Geoscientific Model Development*, *11*(1), 235–255. Retrieved from `https://gmd.copernicus.org/articles/11/235/2018/` doi: 10.5194/gmd-11-235-2018

Boucher, O., Denvil, S., Levavasseur, G., Cozic, A., Caubel, A., Foujols, M.-A., ... Marchand, M. (2022). *Ipcc ddc: Ipsl ipsl-cm6a-lr-inca model output prepared for cmip6 cmip.* World Data Center for Climate (WDCC) at DKRZ. Retrieved from `http://cera-www.dkrz.de/WDCC/ui/Compact.jsp?acronym=C6CMIPILR`

Boucher, O., & Lohmann, U. (1995). The sulfate-CCN-cloud albedo effect. *Tellus*, *47B*(3), 281–300. doi: 10.3402/tellusb.v47i3.16048

Boucher, O., Servonnat, J., Albright, A. L., Aumont, O., Balkanski, Y., Bastrikov, V., ... Vuichard, N. (2020). Presentation and evaluation of the ipsl-cm6a-lr climate model. *Journal of Advances in Modeling Earth Systems*, *12*(7), e2019MS002010. Retrieved from `https://agupubs.onlinelibrary.wiley.com/doi/abs/10.1029/2019MS002010` (e2019MS002010 10.1029/2019MS002010) doi: https://doi.org/10.1029/2019MS002010

Danabasoglu, G., Lamarque, J.-F., Bacmeister, J., Bailey, D. A., DuVivier, A. K., Edwards, J., ... Strand, W. G. (2020). The community earth system model version 2 (cesm2). *Journal of Advances in Modeling Earth Systems*, *12*(2), e2019MS001916. Retrieved from `https://agupubs.onlinelibrary.wiley.com/doi/abs/10.1029/2019MS001916` (e2019MS001916 2019MS001916) doi: https://doi.org/10.1029/2019MS001916

Döscher, R., Acosta, M., Alessandri, A., Anthoni, P., Arsouze, T., Bergman, T., ... Zhang, Q. (2022). The EC-Earth3 Earth system model for the Coupled Model Intercomparison Project 6. *Geoscientific Model Development*, *15*(7), 2973–3020. doi: 10.5194/gmd-15-2973-2022

Dunne, J. P., Horowitz, L. W., Adcroft, A. J., Ginoux, P., Held, I. M., John, J. G., ... Zhao, M. (2020). The GFDL Earth System Model Version 4.1 (GFDL-ESM 4.1): Overall Coupled Model Description and Simulation Characteristics. *Journal of Advances in Modeling Earth Systems*, *12*(11), e2019MS002015. Retrieved from `https://agupubs.onlinelibrary.wiley.com/doi/abs/10.1029/2019MS002015` (e2019MS002015 2019MS002015) doi: https://doi.org/10.1029/2019MS002015

Eyring, V., Bony, S., Meehl, G. A., Senior, C. A., Stevens, B., Stouffer, R. J., & Taylor, K. E. (2016). Overview of the Coupled Model Intercomparison Project Phase 6 (CMIP6) experimental design and organization. *Geosci. Model Dev.*, *9*(5), 1937–1958. doi: 10.5194/gmd-9-1937-2016

Fiedler, S., Kinne, S., Huang, W. T. K., Räisänen, P., O'Donnell, D., Bellouin, N., ... Lohmann, U. (2019). Anthropogenic aerosol forcing – insights from multiple estimates from aerosol-climate models with reduced complexity. *Atmospheric Chemistry and Physics*, *19*(10), 6821–6841. Retrieved from `https://acp.copernicus.org/articles/19/6821/2019/` doi: 10.5194/acp-19-6821-2019

Fiedler, S., Naik, V., O'Connor, F. M., Smith, C. J., Pincus, R., Griffiths, P., ... Forster, P. M. (2023). Interactions between atmospheric composition and climate change – Progress in under-

standing and future opportunities from AerChemMIP, PDRMIP, and RFMIP. *Geoscientific Model Development Discussions*, *2023*, 1–34. doi: 10.5194/gmd-2023-29

Fiedler, S., Stevens, B., & Mauritsen, T. (2017). On the sensitivity of anthropogenic aerosol forcing to model-internal variability and parameterizing a Twomey effect. *J. Adv. Model. Earth Syst.*, *9*, n/a–n/a. doi: 10.1002/2017MS000932

Forster, P. M., Richardson, T., Maycock, A. C., Smith, C. J., Samset, B. H., Myhre, G., ... Schulz, M. (2016). Recommendations for diagnosing effective radiative forcing from climate models for CMIP6. *Journal of Geophysical Research*, *121*(20), 12,460–12,475. doi: 10.1002/2016JD025320

Fouquart, Y., & Bonnel, B. (1980). Computations of solar heating of the Earth's atmosphere: a new parametrization. *Contrib. Atmos. Phys.*, *53*, 35–62.

Ghan, S. J. (2013). Technical note: Estimating aerosol effects on cloud radiative forcing. *Atmospheric Chemistry and Physics*, *13*(19), 9971–9974. Retrieved from https://acp.copernicus.org/articles/13/9971/2013/ doi: 10.5194/acp-13-9971-2013

Golaz, J.-C., Caldwell, P. M., Van Roekel, L. P., Petersen, M. R., Tang, Q., Wolfe, J. D., ... Zhu, Q. (2019). The DOE E3SM Coupled Model Version 1: Overview and Evaluation at Standard Resolution. *Journal of Advances in Modeling Earth Systems*, *11*(7), 2089-2129. Retrieved from https://agupubs.onlinelibrary.wiley.com/doi/abs/10.1029/2018MS001603 doi: https://doi.org/10.1029/2018MS001603

Halthore, R. N., Crisp, D., Schwartz, S. E., Anderson, G. P., Berk, A., Bonnel, B., ... Wiscombe, W. (2005). Intercomparison of shortwave radiative transfer codes and measurements. *Journal of Geophysical Research: Atmospheres*, *110*(D11), n/a–n/a. Retrieved from http://dx.doi.org/10.1029/2004JD005293 (D11206) doi: 10.1029/2004JD005293

Held, I. M., Guo, H., Adcroft, A., Dunne, J. P., Horowitz, L. W., Krasting, J., ... Zadeh, N. (2019). Structure and Performance of GFDL's CM4.0 Climate Model. *Journal of Advances in Modeling Earth Systems*, *11*(11), 3691-3727. Retrieved from https://agupubs.onlinelibrary.wiley.com/doi/abs/10.1029/2019MS001829 doi: https://doi.org/10.1029/2019MS001829

Hourdin, F., Rio, C., Grandpeix, J.-Y., Madeleine, J.-B., Cheruy, F., Rochetin, N., ... Ghattas, J. (2020). Lmdz6a: The atmospheric component of the ipsl climate model with improved and better tuned physics. *Journal of Advances in Modeling Earth Systems*, *12*(7), e2019MS001892. doi: https://doi.org/10.1029/2019MS001892

Kelley, M., Schmidt, G. A., Nazarenko, L. S., Bauer, S. E., Ruedy, R., Russell, G. L., ... Yao, M.-S. (2020). GISS-E2.1: Configurations and Climatology. *Journal of Advances in Modeling Earth Systems*, *12*(8), e2019MS002025. Retrieved from https://agupubs.onlinelibrary.wiley.com/doi/abs/10.1029/2019MS002025 (e2019MS002025 10.1029/2019MS002025) doi: https://doi.org/10.1029/2019MS002025

Kinne, S., O'Donnel, D., Stier, P., Kloster, S., Zhang, K., Schmidt, H., ... Stevens, B. (2013). MAC-v1: A new global aerosol climatology for climate studies. *Journal of Advances in Modeling Earth Systems*, *5*(4), 704–740. doi: 10.1002/jame.20035

Kooperman, G. J., Pritchard, M. S., Ghan, S. J., Wang, M., Somerville, R. C. J., & Russell, L. M. (2012). Constraining the influence of natural variability to improve estimates of global aerosol indirect effects in a nudged version of the Community Atmosphere Model 5. *Journal of Geophysical Research: Atmospheres*, *117*(D23). doi: https://doi.org/10.1029/2012JD018588

Mauritsen, T., Bader, J., Becker, T., Behrens, J., Bittner, M., Brokopf, R., ... Roeckner, E. (2019). Developments in the MPI-M Earth System Model version 1.2 (MPI-ESM 1.2) and its response to increasing CO2. *Journal of Advances in Modeling Earth Systems*, *11*, 998–1038. doi: 10.1029/2018MS001400

Mlawer, E. J., Taubman, S. J., Brown, P. D., Iacono, M. J., & Clough, S. A. (1997). Radiative transfer for inhomogeneous atmospheres: RRTM, a validated correlated-k model for the longwave. *Journal of Geophysical Research: Atmospheres*, *102*(D14), 16663–16682. doi: 10.1029/97JD00237

Neubauer, D., Ferrachat, S., Siegenthaler-Le Drian, C., Stier, P., Partridge, D. G., Tegen, I., ... Lohmann, U. (2019). The global aerosol–climate model ECHAM6. 3–HAM2. 3–Part 2: Cloud evaluation, aerosol radiative forcing, and climate sensitivity. *Geoscientific Model Development*, *12*(8), 3609–3639.

Pincus, R., Forster, P. M., & Stevens, B. (2016). The Radiative Forcing Model Intercomparison Project (RFMIP): experimental protocol for CMIP6. *Geoscientific Model Development*, *9*(9), 3447–3460. doi: 10.5194/gmd-9-3447-2016

Randles, C. A., Kinne, S., Myhre, G., Schulz, M., Stier, P., Fischer, J., ... Lu, P. (2013). Intercomparison of shortwave radiative transfer schemes in global aerosol modeling: results from the AeroCom Radiative Transfer Experiment. *Atmo-*

spheric Chemistry and Physics, *13*(5), 2347–2379. doi: 10.5194/acp-13-2347-2013

Rousset, C., Vancoppenolle, M., Madec, G., Fichefet, T., Flavoni, S., Barthélemy, A., ... Vivier, F. (2015). The louvain-la-neuve sea ice model lim3.6: global and regional capabilities. *Geosci. Model Dev.*, *8*, 2991–3005. doi: 10.5194/gmd-8-2991-2015

Séférian, R., Baek, S., Boucher, O., Dufresne, J.-L., Decharme, B., Saint-Martin, D., & Roehrig, R. (2018). An interactive ocean surface albedo scheme: Formulation and evaluation in two atmospheric models. , *11*, 321–338.

Seland, Ø., Bentsen, M., Olivié, D., Toniazzo, T., Gjermundsen, A., Graff, L. S., ... Schulz, M. (2020). Overview of the Norwegian Earth System Model (NorESM2) and key climate response of CMIP6 DECK, historical, and scenario simulations. *Geoscientific Model Development*, *13*(12), 6165–6200. Retrieved from https://gmd.copernicus.org/articles/13/6165/2020/ doi: 10.5194/gmd-13-6165-2020

Sellar, A. A., Jones, C. G., Mulcahy, J. P., Tang, Y., Yool, A., Wiltshire, A., ... Zerroukat, M. (2019). UKESM1: Description and Evaluation of the U.K. Earth System Model. *Journal of Advances in Modeling Earth Systems*, *11*(12), 4513-4558. Retrieved from https://agupubs.onlinelibrary.wiley.com/doi/abs/10.1029/2019MS001739 doi: https://doi.org/10.1029/2019MS001739

Smith, C. J., Kramer, R. J., Myhre, G., Alterskjær, K., Collins, W., Sima, A., ... Forster, P. M. (2020). Effective radiative forcing and adjustments in cmip6 models. *Atmospheric Chemistry and Physics*, *20*(16), 9591–9618. Retrieved from https://acp.copernicus.org/articles/20/9591/2020/ doi: 10.5194/acp-20-9591-2020

Stevens, B., Fiedler, S., Kinne, S., Peters, K., Rast, S., Müsse, J., ... Mauritsen, T. (2017). MACv2-SP: a parameterization of anthropogenic aerosol optical properties and an associated Twomey effect for use in CMIP6. *Geosci. Mod. Dev.*, *10*(1), 433–452. doi: 10.5194/gmd-10-433-2017

Stevens, B., Giorgetta, M., Esch, M., Mauritsen, T., Crueger, T., Rast, S., ... Roeckner, E. (2013). Atmospheric component of the MPI-M Earth System Model: ECHAM6. *Journal of Advances in Modeling Earth Systems*, *5*(2), 146–172. doi: 10.1002/jame.20015

Swart, N. C., Cole, J. N. S., Kharin, V. V., Lazare, M., Scinocca, J. F., Gillett, N. P., ... Winter, B. (2019). The Canadian Earth System Model version 5 (CanESM5.0.3). *Geoscientific Model Development*, *12*(11), 4823–4873. Retrieved from https://gmd.copernicus.org/articles/12/4823/2019/ doi: 10.5194/gmd-12-4823-2019

Séférian, R., Nabat, P., Michou, M., Saint-Martin, D., Voldoire, A., Colin, J., ... Madec, G. (2019). Evaluation of cnrm earth system model, cnrm-esm2-1: Role of earth system processes in present-day and future climate. *Journal of Advances in Modeling Earth Systems*, *11*(12), 4182-4227. Retrieved from https://agupubs.onlinelibrary.wiley.com/doi/abs/10.1029/2019MS001791 doi: https://doi.org/10.1029/2019MS001791

Tatebe, H., Ogura, T., Nitta, T., Komuro, Y., Ogochi, K., Takemura, T., ... Kimoto, M. (2019). Description and basic evaluation of simulated mean state, internal variability, and climate sensitivity in MIROC6. *Geoscientific Model Development*, *12*(7), 2727–2765. Retrieved from https://gmd.copernicus.org/articles/12/2727/2019/ doi: 10.5194/gmd-12-2727-2019

Twomey, S. (1974). Pollution and the planetary albedo. *Atmos. Environ.*, *8*, 1251-1256.

van Noije, T., Bergman, T., Sager, L., P., O'Donnell, D., Makkonen, R., ... Yang, S. (2021). Ec-earth3-aerchem: a global climate model with interactive aerosols and atmospheric chemistry participating in cmip6. *Geosci. Model Dev.*, *14*, 5637–5668. doi: 10.5194/gmd-14-5637-2021

Voldoire, A., Saint-Martin, D., Sénési, S., Decharme, B., Alias, A., Chevallier, M., ... Waldman, R. (2019). Evaluation of CMIP6 DECK Experiments With CNRM-CM6-1. *Journal of Advances in Modeling Earth Systems*, *11*(7), 2177-2213. Retrieved from https://agupubs.onlinelibrary.wiley.com/doi/abs/10.1029/2019MS001683 doi: https://doi.org/10.1029/2019MS001683

Williams, K. D., Copsey, D., Blockley, E. W., Bodas-Salcedo, A., Calvert, D., Comer, R., ... Xavier, P. K. (2018). The Met Office Global Coupled Model 3.0 and 3.1 (GC3.0 and GC3.1) Configurations. *Journal of Advances in Modeling Earth Systems*, *10*(2), 357-380. Retrieved from https://agupubs.onlinelibrary.wiley.com/doi/abs/10.1002/2017MS001115 doi: https://doi.org/10.1002/2017MS001115

Wu, T., Zhang, F., Zhang, J., Jie, W., Zhang, Y., Wu, F., ... Hu, A. (2020). Beijing climate center earth system model version 1 (bcc-esm1): model description and evaluation of aerosol simulations. *Geoscientific Model Development*, *13*(3), 977–1005. Retrieved from https://gmd.copernicus.org/articles/13/977/2020/ doi: 10.5194/gmd-13-977-2020

Wyser, K., van Noije, T., Yang, S., von Hardenberg, J.,

O'Donnell, D., & Döscher, R. (2020). On the increased climate sensitivity in the ec-earth model from cmip5 to cmip6. *Geosci. Model Dev.*, *13*, 3465–3474. doi: 10.5194/gmd-13-3465-2020

Yukimoto, S., Kawai, H., Koshiro, T., Oshima, N., Yoshida, K., Urakawa, S., ... Ishii, M. (2019). The meteorological research institute earth system model version 2.0, mri-esm2.0: Description and basic evaluation of the physical component. *Journal of the Meteorological Society of Japan. Ser. II*, *97*(5), 931-965. doi: 10.2151/jmsj.2019-051

Ziehn, T., Chamberlain, M. A., Law, R. M., Lenton, A., Bodman, R. W., Dix, M., ... Srbinovsky, J. (2020). The australian earth system model: Access-esm1.5. *Journal of Southern Hemisphere Earth Systems Science*, *70*(1), 193–214. Retrieved from `https://doi.org/10.1071/ES19035`

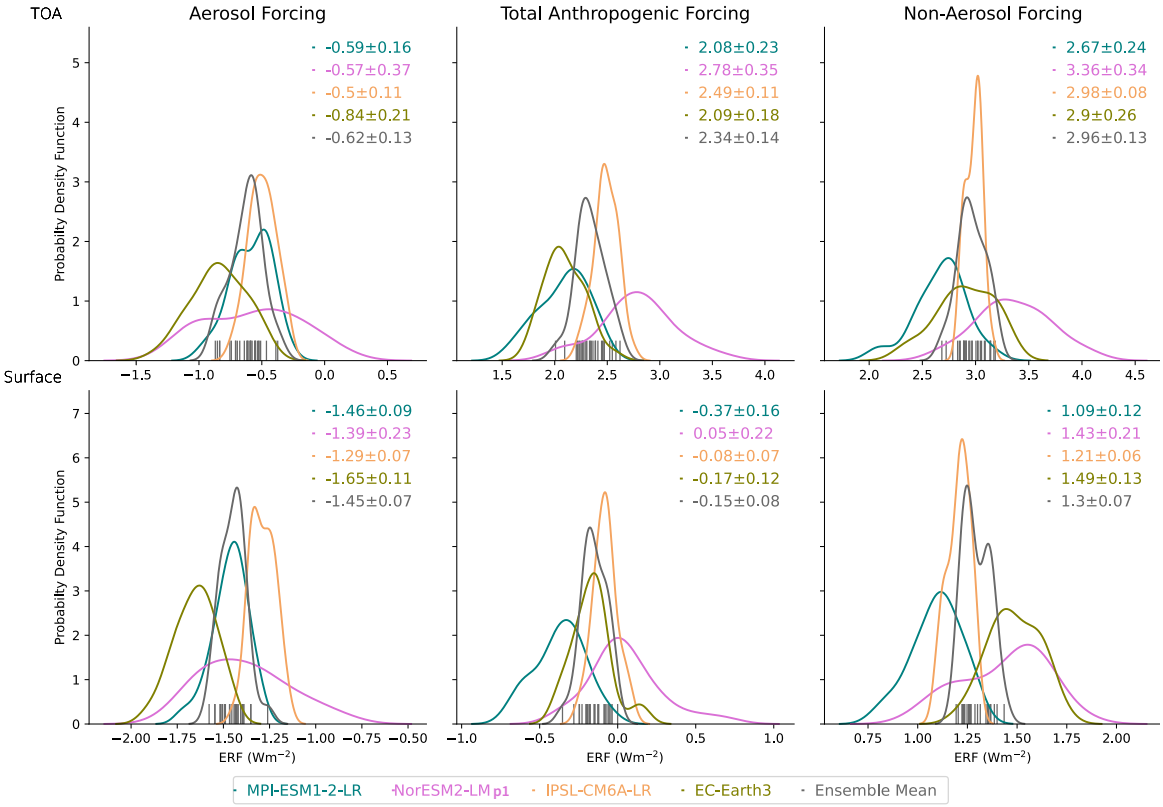

Figure S1. Annual global ERF estimates for 2014 against 1850 from RFMIP-SpAer. Shown are (left to right) aerosol ERF, total anthropogenic ERF, and total anthropogenic minus aerosol ERF (top) at TOA and (bottom) the surface for the color-coded models. The multi-model ensemble statistic is shown as gray line and rug plot. Values printed at the top are the global mean ± the year-to-year standard deviation. We include here all available *piClim* experiments from RFMIP-SpAer at the time of analysis for sampling the variability, i.e., 60 years of *piClim-SpAer-aer* from EC-Earth3, 150 years from IPSL-CM6A-LR, 90 years from MPI-ESM1-2-LR, and 30 years from NorESM2-LM (here p1). The means here therefore slightly differ from the ones in Figure 1. Note the different x-axes.

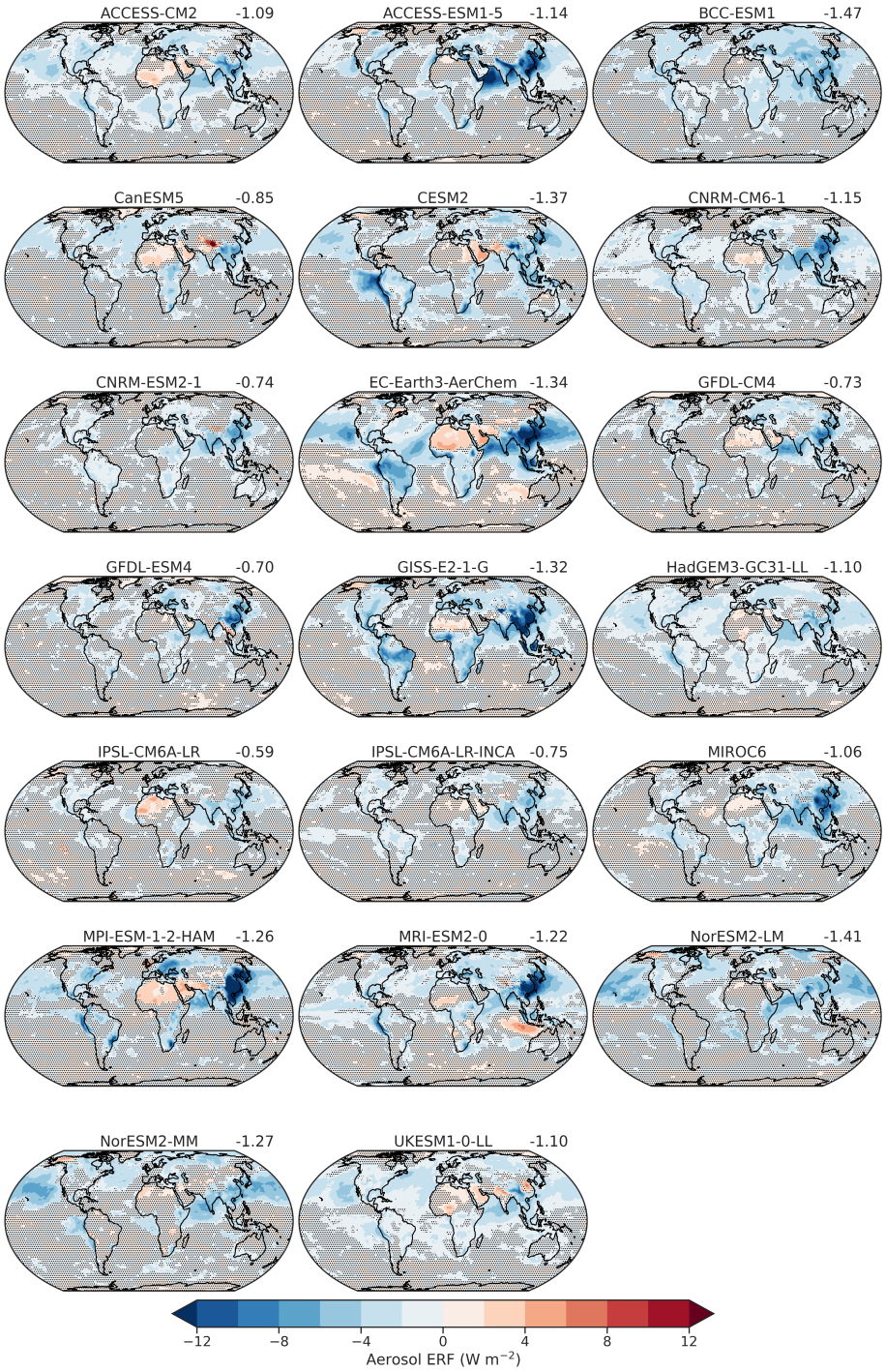

Figure S2. Spatial patterns of present-day aerosol effective radiative effects of all available models in RFMIP-ERF. Values in the corner are the global means in Wm^{-2}. We show the models listed in Table S2, and for NorESM2-LM the p2 configuration. Values in the corner are the global means and areas without statistically significant values (p-value 0.05) are masked with black dots.

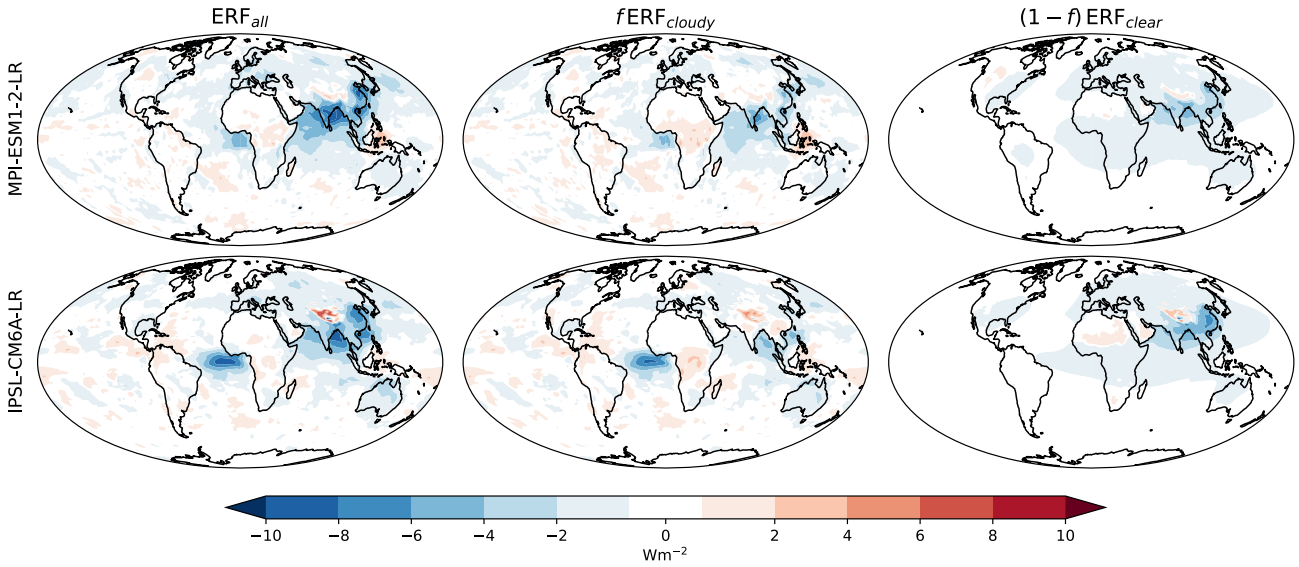

Figure S3. Net contribution of clear and cloudy sky to aerosol $\mathcal{F}$ at TOA in RFMIP-SpAer. Shown are net contributions from clear sky, (1-f)$\mathcal{F}_{clear}$, and cloudy sky, f $\mathcal{F}_{cloudy}$, to the all-sky aerosol radiative effects, $\mathcal{F}_{all}$, at the top of the atmosphere (TOA) for MPI-ESM1.2-LR and IPSL-CM6A-LR using identical anthropogenic aerosol optical properties and associated effects on the cloud droplet number concentration. All values are calculated from the output of RFMIP-SpAer experiments *piClim-SpAer-aer* against *piClim-control* by applying equation 4.

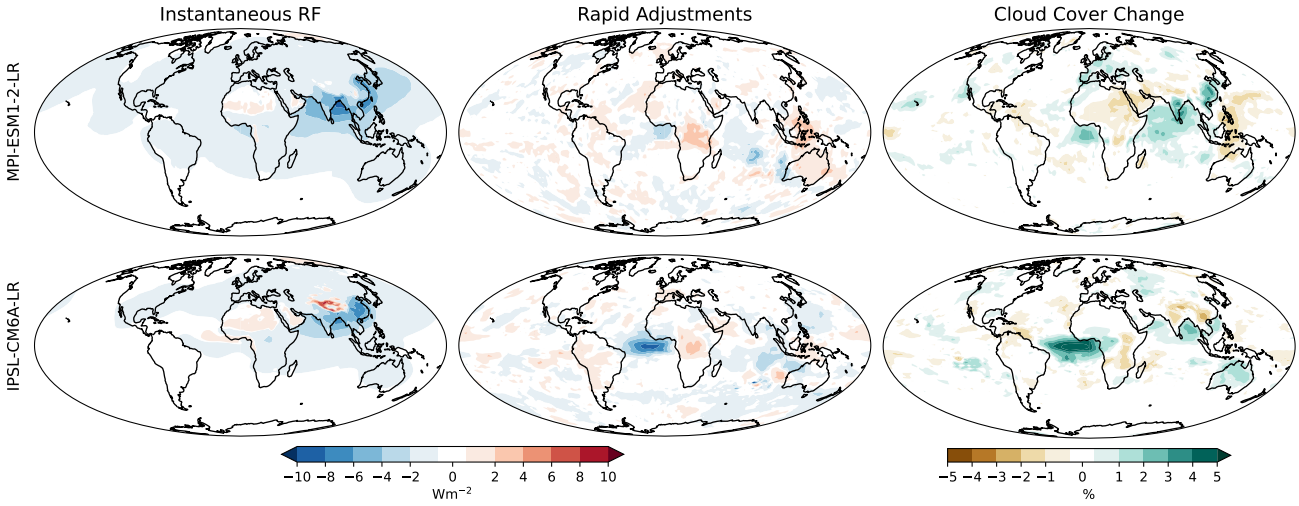

Figure S4. Contributions from $\mathcal{I}$ and $\mathcal{A}$ to aerosol $\mathcal{F}$. Shown are (left to right) the instantaneous radiative effects, $\mathcal{I}$, and the net contribution from adjustments, $\mathcal{A}$, for shortwave radiation at TOA for all sky conditions, and the change in cloud cover, Δf, between the *piClim-SpAer-aer* and *piClim-control*. Results are calculated with equation 5 using double-call diagnostics for anthropogenic aerosols to determine $\mathcal{I}$.

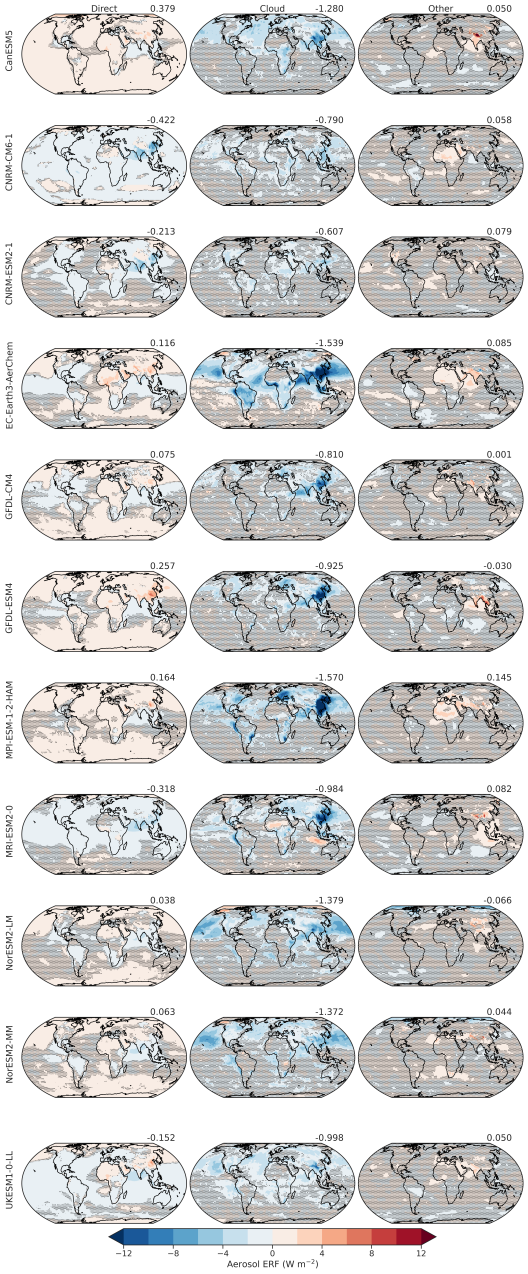

Figure S5. Spatial patterns of the process contributions to the present-day aerosol effective radiative effects in all models with the necessary diagnostic output in RFMIP-ERF. Shown are (left to right) direct effects, cloud-mediated effects, and residual effects following the method from Ghan (2013). Values in the corner are the global means in Wm^{-2}. We show the configuration NorESM2-LM p2. Values in the corner are the global means and areas without statistically significant values (p-value 0.05) are masked with black dots.

Table S1. CMIP6 models contributing historical atmosphere-only experiments for 1850–2014 to RFMIP (*piClim-hist*), used for the time series of ERF in Fig. 1. Trends for the aerosol and total ERF are listed for the periods 1930–1960 and 2000–2014 in Wm^{-2} per year, calculated as linear regressions.

Model name	**Reference**	**Aerosol 1930–1960** $[Wm^{-2}yr^{-1}]$	**Aerosol 2000–2014** $[Wm^{-2}yr^{-1}]$	**Total 1930–1960** $[Wm^{-2}yr^{-1}]$	**Total 2000–2014** $[Wm^{-2}yr^{-1}]$
CanESM5	Swart et al. (2019)	-0.012	0.007	0.003	0.039
CNRM-CM6-1	Voldoire et al. (2019)	-0.009	0.002	-0.001	0.029
E3SM	Golaz et al. (2019)	-0.019	0.010	-	-
GFDL-CM4	Held et al. (2019)	-0.010	0.019	0.004	0.050
GFDL-ESM4	Dunne et al. (2020)	-0.011	0.021	-	-
GISS-E2-1-G	Kelley et al. (2020)	-0.015	0.001	0.002	0.025
HadGEM3-GC31-LL	Williams et al. (2018)	-0.013	0.009	-0.003	0.037
IPSL-CM6A-LR	Boucher et al. (2020)	-0.007	0.018	0.008	0.032
MIROC6	Tatebe et al. (2019)	-0.009	-0.001	0.008	0.025
MPI-ESM1-2-LR	Mauritsen et al. (2019)	-0.007	-0.002	0.006	0.029
MRI-ESM2-0	Yukimoto et al. (2019)	-0.018	0.001	-	-
NorESM2-LM	Seland et al. (2020)	-0.016	-0.009	0.005	0.051
UKESM1-0-LL	Sellar et al. (2019)	-0.028	0.018	-	-
Median		-0.012	0.007	0.004	0.032
Mean ± Std. Dev.		-0.013±0.005	0.007±0.008	0.004±0.003	0.035±0.008

Table S2. Aerosol ERF in (top block) RFMIP-SpAer and (bottom block) RFMIP-ERF, based on the thirty-year-long experiments from the models listed under Experiment ID.

Model name	**Reference**	**Experiment ID**	**Aerosol ERF [$\mathbf{Wm^{-2}}$]**
EC-Earth3 *	Döscher et al. (2022)	r2i1p1f1	-0.79
IPSL-CM6A-LR *	Boucher et al. (2020)	r1i1p1f1	-0.46
MPI-ESM1-2-LR *	Mauritsen et al. (2019)	r1i1p1f1	-0.52
NorESM2-LM p1 *	Seland et al. (2020)	r1i1p1f1	-0.55
NorESM2-LM p2 *	Seland et al. (2020)	r1i1p2f1	-0.53
ACCESS-CM2	Bi et al. (2020)	r1i1p1f1	-1.09
ACCESS-ESM1-5 *	Ziehn et al. (2020)	r1i1p1f1	-1.14
BCC-ESM1 *	Wu et al. (2020)	r1i1p1f1	-1.47
CanESM5	Swart et al. (2019)	r1i1p2f1	-0.85
CESM2	Danabasoglu et al. (2020)	r1i1p1f1	-1.37
CNRM-CM6-1	Voldoire et al. (2019)	r1i1p1f2	-1.15
CNRM-ESM2-1	Séférian et al. (2019)	r1i1p1f2	-0.74
EC-Earth3-AerChem *	van Noije et al. (2021)	r1i1p1f1	-1.34
GFDL-CM4	Held et al. (2019)	r1i1p1f1	-0.73
GFDL-ESM4	Dunne et al. (2020)	r1i1p1f1	-0.70
GISS-E2-1-G	Kelley et al. (2020)	r1i1p1f1	-1.32
HadGEM3-GC31-LL	Williams et al. (2018)	r1i1p1f3	-1.10
IPSL-CM6A-LR	Boucher et al. (2020)	r1i1p1f1	-0.59
IPSL-CM6A-LR-INCA *	Boucher et al. (2022)	r1i1p1f1	-0.75
MIROC6	Tatebe et al. (2019)	r1i1p1f1	-1.06
MPI-ESM1-2-HAM *	Neubauer et al. (2019)	r1i1p1f1	-1.26
MRI-ESM2-0	Yukimoto et al. (2019)	r1i1p1f1	-1.21
NorESM2-LM p1	Seland et al. (2020)	r1i1p1f1	-1.21
NorESM2-LM p2 *	Seland et al. (2020)	r1i1p2f1	-1.41
NorESM2-MM	Seland et al. (2020)	r1i1p1f1	-1.27
UKESM1-0-LL	Sellar et al. (2019)	r1i1p1f4	-1.10

* *piClim(-aer)* experiments of these models became newly available in RFMIP after the publication by Smith et al. (2020).

Table S3. Contributions to aerosol ERF in RFMIP-ERF. Shown are the contributions from direct, cloud-mediated, and other effects to the present-day aerosol ERF following Ghan (2013) The unitless aerosol optical properties listed are the PI to PD change in the aerosol optical depth at 550 nm, $\Delta\tau$, the absorption aerosol optical depth, τ_{abs}, for PD, the fraction of natural to anthropogenic τ_{abs}, $\frac{\tau_{abs}(nat)}{\tau_{abs}(ant)}$, for PD, the single scattering albedo of anthropogenic aerosols, $\omega_0(ant)$, for PD, and the mass absorption coefficient (MAC) for black carbon (BC) for PD (all) and the anthropogenic share (ant) based on available model output. All data are from the models listed in Tab. S2

Model name	**Direct** [Wm^{-2}]	**Cloud-mediated** [Wm^{-2}]	**Other** [Wm^{-2}]	$\Delta\tau$	τ_{abs}	$\frac{\tau_{abs}(nat)}{\tau_{abs}(ant)}$	$\omega_0(ant)$	MAC ant (total) BC [m^2g^{-1}]	BC load [$10^{-7}kgm^{-2}$]
ACCESS-CM2	-	-	-	0.04	0.006	1.16	0.92	-	-
ACCESS-ESM1-5 *	-	-	-	0.02	-	-	-	-	-
CanESM5	0.38	-1.28	0.05	0.04	0.014	0.66	0.77	-	-
CESM2	-	-	-	0.01	0.007	1.15	0.76	20.47	3.27
CNRM-CM6-1	-0.42	-0.79	0.06	0.02	0.003	1.85	0.94	-	-
CNRM-ESM2-1	-0.21	-0.61	0.08	0.02	0.003	1.66	0.93	-	-
EC-Earth3-AerChem *	0.12	-1.54	0.08	0.04	0.006	0.61	0.89	12.05 (14.23)	4.44
GFDL-CM4	0.08	-0.81	0.001	0.04	0.008	1.04	0.90	19.34 (28.62)	2.85
GFDL-ESM4	0.26	-0.92	-0.03	0.04	0.0098	0.86	0.87	16.97 (24.14)	4.08
GISS-E2-1-G	-	-	-	0.05	-	-	-	-	-
HadGEM3-GC31-LL	-	-	-	0.04	0.006	1.13	0.92	-	-
IPSL-CM6A-LR	-	-	-	0.03	0.003	2.3	0.97	-	-
IPSL-CM6A-LR-INCA *	-	-	-	0.04	0.003	3.34	0.98	-	-
MIROC6	-	-	-	0.03	0.002	0.98	0.96	2.01 (6.41)	2.70
MPI-ESM1-2-HAM *	0.16	-1.57	0.14	0.03	0.004	1.13	0.93	9.98 (12.34)	3.13
MRI-ESM2-0	-0.32	-0.98	0.08	0.03	0.006	2.07	0.95	-	-
NorESM2-LM p1	0.03	-1.21	-0.03	0.02	0.004	1.01	0.92	-	-
NorESM2-LM p2 *	0.04	-1.38	-0.07	0.02	0.004	1.00	0.92	8.22 (12.07)	3.07
NorESM2-MM	0.06	-1.37	0.04	0.02	0.004	1.02	0.91	8.19 (12.15)	3.20
UKESM1-0-LL	-0.15	-1.00	0.05	0.03	0.006	1.02	0.91	18.56 (20.42)	3.06

* *piClim(-aer)*experiments of these models became newly available in RFMIP-ERF after the publication by Smith et al. (2020).